Dynamic vortex ordering in thin a-Nb70Ge30 films

Geers, J.M.E.; Attanasio, C.; Hesselberth, M.B.S.; Aarts, J.; Kes, P.H.

Dynamic vortex ordering in thin a-$Nb_{70}Ge_{30}$ films

J. M. E. Geers, C. Attanasio*, M. B. S. Hesselberth, J. Aarts,† and P. H. Kes
Kamerlingh Onnes Laboratory, Leiden University, P.O. Box 9504, 2300 RA Leiden, the Netherlands
(Received 16 August 2000; published 9 February 2001)

We investigated ordering of the vortex lattice under the influence of a driving current in amorphous superconducting films of $Nb_{70}Ge_{30}$ with varying amounts of disorder. Using the nonlinear behavior of the voltage versus current relations, i.e., the peak in the dynamical resistance, we map the occurrence of this dynamical ordering (DO) in the (B,T) phase diagram. Using the collective pinning analysis, DO is shown to appear when the size of the correlated regions drops below the order of $\approx$ ten times the vortex lattice distance. This means that for weaker intrinsic disorder, DO moves closer to the melting line. The current at which DO occurs diverges at the melting transition, in agreement with the notion that increasing velocities are needed to overcome the effect of either temperature or softening of the shear modulus of the vortex lattice.

DOI: 10.1103/PhysRevB.63.094511 PACS number(s): 74.60.Ge, 74.60.Jg, 74.76.Db

I. INTRODUCTION

Vortices start to move if the Lorentz force exceeds the pinning force F_p. The way this exactly happens depends on the amount of disorder in the lattice. If the disorder is weak, a correlated volume V_c can be defined in which all vortices are pinned collectively and start to move at one specific threshold value of F_p. The concept of collective pinning (CP) was introduced by Larkin and Ovchinnikov[1] and experimentally confirmed by experiments on weakly pinning amorphous (a-)Nb_3Ge, a-Nb_3Si, and a-Mo_3Si films[2,3] and on 2H-$NbSe_2$ crystals.[4] Since V_c in these cases can be large, all vortices have approximately the same velocity, which increases by increasing the driving force. This type of motion can be called elastic flow. The amount of defects in the sliding solid is small.

With stronger disorder, different vortices feel different pinning forces. In consequence, some vortices start to move around pinned regions and with increasing driving force, more vortices take part in the motion. The moving structure is strongly defective and spatially inhomogeneous, and the dissipation is high. However, if driving force and velocity are increased over some threshold, the number of defects can decrease quite suddenly and a homogeneous moving lattice appears. As will be discussed below, one signature of such a transition is a superlinear $V(I)$ characteristic, equivalent to a peak in the differential resistance R_d. This healing or dynamic ordering (DO) phenomenon is the subject of this paper. Specifically, we want to investigate under which conditions the direct transition from a pinned lattice to a sliding solid changes into a transition with an intermediate plastic flow state and DO. For this we used a series of thin-film samples of a-$Nb_{70}Ge_{30}$. In principle, such amorphous materials are weakly pinning, but the amount of disorder can be increased by choosing different deposition conditions. The samples range in thickness from 35 to 300 nm and the vortex lattice is two-dimensional (2D) down to the lowest studied temperature, which means that the collective volume V_c is cylindrical and equals $R_c^2 d$, with R_c the radius and d the film thickness. The occurrence of channel-like flow as indicated by a peak in R_d is mapped on the (B,T) phase diagram. Very generally, we find that the peak, and therefore the DO, occurs for $R_c/a_0 \leqslant 10$ (with a_0 the intervortex distance). For weak disorder, this condition is only found very close to the melting line, while increasing the disorder broadens the range substantially. Also, we find that the current needed to induce DO strongly increases near the melting line, in good agreement with the theoretical prediction by Koshelev and Vinokur.[6]

II. DYNAMIC ORDERING

That the number of dislocations in a disordered vortex lattice decreases suddenly at high currents was first found in 2D molecular dynamics studies at $T=0$ by Shi and Berlinsky.[5] More recently, Koshelev and Vinokur[6] investigated the behavior at finite temperatures, both analytically and on the basis of simulations (see also Ref. 7). For strong disorder, they found that at every temperature below the thermodynamic melting temperature T_m a driving force density F_{do} can be found at which disorderly moving vortices crystallize into a more or less perfect lattice. The temperature dependence of F_{do} close to T_m is given by

$$F_{do} = \frac{1}{4\sqrt{2\pi}} \frac{n_v \Gamma}{k_B (T_m - T) d r_p^3} \ [\mathrm{N/m^3}], \tag{1}$$

where Γ is a measure for the disorder strength, n_v is the vortex areal density, r_p is the range of the elementary pinning interaction, and T_m is the 2D melting temperature. DO occurs if F_{do} is larger than the pinning force density F_p. Physically, Eq. (1) can be understood through the concept of a ''shaking temperature'' T_{sh}, which should be viewed as energy generated by the nonuniform motion of the vortices through the disorder potential, and is inversely proportional to the velocity. At $T=0$ it follows that the effective temperature of the vortex system in motion $T_{\mathrm{eff}} = T + T_{sh} = T_{sh}$, so that the ordering force is reached when T_{sh} falls below T_m. With increasing T, it needs increasing velocities for T_{eff} to drop below T_m, which explains the divergence of F_{do} for $T \rightarrow T_m$.

Also studied was the average vortex velocity v_v against driving force F_{ex}, which is equivalent to a $V(I)$ characteristic. The simulations showed a sharp increase of v_v (or V) around F_{do} (or I), which would translate in a peak in the

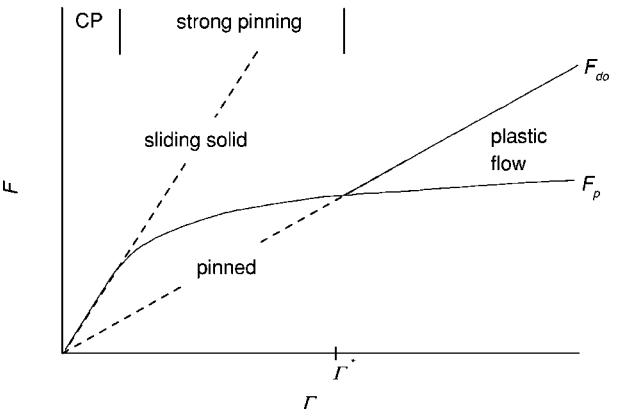

FIG. 1. Dynamic ordering force F_{do} and pinning force F_p versus the disorder parameter Γ as calculated in by Faleski *et al.*[8]

differential resistance R_d. In similar 2D molecular dynamics studies at $T=0$ Faleski *et al.*[8] investigated more closely the various types of flow for different amounts of disorder. The results can be discussed in terms of a force-disorder diagram as shown in Fig. 1. It contains three regimes. For low Γ the transition from pinning to flux flow follows $F_p \propto \Gamma$, which is the Larkin-Ovchinnikov CP regime. When CP breaks down ($R_c \sim a_0$), individual strong pinning leads to $F_p \propto \sqrt{\Gamma}$. The transition is still elastic, since $F_p > F_{do}$ [with F_{do} given by Eq. (1) at $T=0$] so that defects are healed immediately. However, since $F_{do} \propto \Gamma$, a third regime is possible where depinning takes place without reordering of the lattice. The flow is plastic, and DO takes place at F_{do} ($>F_p$). The simulations give more insight in the motion in this regime. At F_p the velocity distribution is bimodal: a fraction n_s of the vortices (the slow ones) is not moving ($v_s \approx 0$), while another fraction n_f (the fast ones) is at a finite velocity v_f ($n_s + n_f = 1$). The average drift velocity can be estimated by $v_d = n_s v_s + n_f v_f$. In the plastic flow regime the amount of defects in the moving lattice is large, but decreases under influence of the driving force F_{ex}. If F_{ex} is increased, first the fraction n_f of fast moving vortices increases rapidly. Then, when at high enough F_{ex} the slow fraction n_s has almost reduced to zero, the velocity v_f starts to increase. Almost all vortices are moving now with the same velocity and less defects can exist. This is dynamic ordering. The change from a bimodal to single-mode velocity distribution gives rise to a peak in the dynamical resistance:

$$(dv_d/dF_{ex}) \approx dv_f/dF_{ex} + (dn_f/dF_{ex})(v_f - v_s). \quad (2)$$

Below the peak the slow vortices are essentially not moving ($v_s \approx 0$) while the number n_f of fast vortices is increasing rapidly, leading to a superlinear $V(I)$. Above the peak the rate dn_f/dF_{ex} at which the slow vortex fraction decreases and the fast vortex fraction increases slows down considerably, while $(v_f - v_s) \sim F_{ex}$. It is this slowing down of the rate dn_f/dF_{ex} with increasing F_{ex} that is responsible for the peak in the differential resistance.

So DO only takes place in a plastically moving lattice, for which a certain minimum amount of disorder is necessary. The amount of disorder depends on the pinning mechanisms and on the strength of the vortex interactions, and is therefore field and temperature dependent. Generally, the elastic pinning length R_c/a_0 decreases above some field and the disorder increases. It becomes especially large close to the melting line where the lattice is very soft. Therefore, close to the melting line, DO should always take place. But also at low fields the lattice is soft and the disorder can be large. Dynamic ordering, however, does not necessarily occur at low fields since F_p is large here and the ordering force F_{do} might be smaller than F_p even for large intrinsic disordered samples.

On the experimental side, for thin films of *a*-MoGe, peaks in R_d were reported by Hellerqvist *et al.*[9] and by Hellerqvist and Kapitulnik,[10] and interpreted in terms of DO. They did not attempt, however, to connect occurrence of DO and disorder in a systematic way, which is the purpose of this paper. For completeness, an earlier report[11] showing peaks in R_d for thick *a*-MoGe films should also be mentioned. Another much studied system is 2H-$NbSe_2$, where the vortex lattice is 3D. DO was found close to the melting line by transport measurements,[12] and in decoration[13] and neutron-diffraction[14] experiments. Due to the extreme weakness of the pinning also related phenomena occur, such as metastability and history dependence.[15,16]

III. EXPERIMENTAL

Thin-film *a*-$Nb_{70}Ge_{30}$ samples of varying thickness on Si (001) substrates with a 200-nm-thick artificial SiO_2 top layer were prepared in two different sputtering systems. The first system is an ultra high vacuum (UHV) system with a base pressure better than 10^{-9} mbar. Sputtering is multitarget dc magnetron sputtering with 6×10^{-3}-mbar argon as sputtering gas. During sputtering the samples are not cooled in this system. The other system is a Leybold Z400 sputtering system with a base pressure of $\sim 10^{-6}$ mbar. Sputtering is rf diode sputtering from a composite target with approximately 6×10^{-3}-mbar Ar as sputtering gas. During sputtering the substrate holder is water cooled.

The temperature at which sputtering takes place is very important for the pinning properties of the samples. A small increase in deposition temperature (estimated at no more than 30 K) causes a much broader distribution in pinning potentials and therefore less collective pinning behavior. For the samples from the UHV system, the disorder also increases with film thickness, probably due to more heating in the longer sputtering period. High-resolution electron microprobe (HREM) analysis, however, shows that all samples are amorphous and do not show (micro)crystallites.

In the UHV system samples were prepared ranging in thickness from 38 to 300 nm. Electron microprobe analysis (EPMA) on these samples shows a composition of 70% Nb and 30% Ge. The not-cooled samples from the UHV system will be indicated as **U** followed by a number giving the film thickness in nanometers. The cooled samples from the Z400 ranging in thicknesses between 34 and 190 nm will be indicated with **Z** and a number. These samples have a composition of 67% Nb and 33% Ge. One sample was specially prepared to make it weakly pinning by sputtering in short

TABLE I. Sample parameters. For all samples $\Delta T \sim 20$ mK.

Series	d (nm)	ρ_0 ($\mu\Omega$ cm)	T_c (K)	S (T/K)	κ	$\xi(0)$ (nm)
U	38	222	3.1	2.0	73	7.4
	75	223	3.1	1.9	72	7.5
	150	263	3.1	2.0	81	7.3
	225	247	3.1	2.15	81	7.1
	300	286	3.1	2.2	83	6.9
Z	34	247	2.9	2.1	81	7.4
	67	252	2.9	2.0	79	7.5
	130	245	2.9	2.0	78	7.5
W	190	230	3.1	2.0	76	8.8

cycles (30-s sputtering, 2-min cool down). It will be called **W**190. It was made from a different target and its composition was 70% Nb and 30% Ge. After sputtering, the samples were ion etched in 100μm-wide strips. The strips have a total length of 3 mm and a distance between the voltage contacts of 1.5 mm.

Ac-resistance measurements were performed as function of temperature and magnetic field $[R_{ac}(B,T)]$. For these measurements a current density of $J_{ac} \leqslant 5000$ A/m^2 ($\ll J_c$) was used. Voltage (V) versus current (I) relations were measured by stepwise increasing the magnitude of the current. Current commutation and averaging was used to compensate for thermal voltages. Occasionally $V(I)$ was measured without commutations, but no differences were observed. Also hysteresis was never observed. The dynamical resistance R_d was calculated from the dc measurements using a standard three-point differentiation algorithm. Since the $V(I)$ measurements were performed up to high current densities ($J \sim 10^9$ A/m^2), care had to be taken to prevent heating and the samples were immersed directly in liquid helium.

IV. SAMPLE CHARACTERISTICS

All samples from the **U** series have $T_c = 3.1$ K and a transition width in zero field of the order of $\Delta T_c \sim 20$ mK. The resistivity at $T = 5$ K is $\rho_n \approx 230$ $\mu\Omega$cm. The **Z** series have $T_c = 2.9$ K and $\Delta T_c \sim 20$ mK. For these samples $\rho_n(T=5\ \text{K}) = 250$ $\mu\Omega$ cm. **W190** has $T_c = 3.1$ K and $\rho_n(T=5\ \text{K}) = 230$ $\mu\Omega$ cm. The sample characteristics are given in Table I.

For weakly collective pinning samples it has been shown how to determine the upper critical field B_{c2} from $R(B)$ measurements.[17] For this type of samples it has also been demonstrated that 2D Kosterlitz-Thouless (2D KT) melting takes place before thermal depinning. The melting field B_m can be determined both from $R(B)$ and from $V(I)$ measurements. For the more strongly disordered samples of this work, $R(B)$ and $V(I)$ look differently. Therefore the way to determine B_{c2} is not directly clear. Moreover, the occurrence of 2D KT melting in these films is not *a priori* established. It could be that the vortex lattice is too much disordered and the correlated domains too small for KT melting to take place. In this section we will show how we derived $B_{c2}(T)$ and $B_m(T)$ from our $R_{ac}(B)$ measurements. The good correspondence between the experimentally determined values and the theoretical curves is an indication that B_{c2} and B_m are determined correctly and that melting via unbinding of dislocation pairs still takes place. Later on, we will give an indication for the size of the correlated regions.

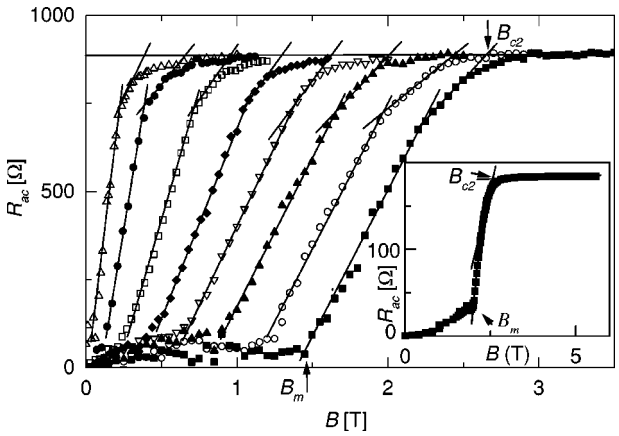

FIG. 2. Ac resistance R_{ac} versus field magnetic field B measured with $J_{ac} = 3000$ A/m^2 for **U38** at temperatures of $T = 1.7$, 1.9, 2.1, 2.3, 2.5, 2.7, 2.9, and 3.0 K (right to left). The determination of B_{c2} and B_m is indicated. Inset: $R_{ac}(B)$ for **W190** measured with $J_{ac} = 2500$ A/m^2 at $T = 1.68$ K.

The more strongly disordered samples of this work show behavior as indicated in Fig. 2 for **U38** and **W190**. The measurements have been performed with $J_{ac} \leqslant 5000$ A/m^2. In the main figure $R_{ac}(B)$ is plotted for **U38** at temperatures ranging from $T = 1.7$ K to $T = 3.0$ K. In the inset $R_{ac}(B)$ is plotted for **W190** at $T = 1.68$ K. All curves show a linear region and then a clear kink in slope followed by a curved region at higher fields. At low fields $R_{ac}(B)$ does not drop sharply to zero, but decreases much more slowly than for weakly pinning samples. For **W190** $R_{ac}(B)$ shows a minimum and maximum.

We now argue that the measured curves can be interpreted as follows. The linear regions in $R_{ac}(B)$ correspond to more and more vortices depinning. The behavior in the curved regions at high fields is dominated by fluctuations and inhomogeneities. We have tried fluctuation analysis to determine B_{c2}[18] but this did not work well due to the large amount of inhomogeneities. Values for B_{c2} can be obtained by extrapolating the data just above the kink, where all vortices are moving, linearly to R_n. This is justified on basis of the work by Larkin and Ovchinnikov who described the full flux flow resistance R_f close to B_{c2} as

$$R_f/R_n \approx 1 - \alpha(T)(1 - B/B_{c2}). \tag{3}$$

A strong indication that B_{c2} is determined correctly in this way follows from its temperature dependence, which is described in the implicit relation[19]

$$\ln(T/T_c) = \Psi\left(\frac{1}{2}\right) - \Psi\left(\frac{1}{2} + \frac{4\xi(0)^2 T_c B_{c2}(T)}{\pi \phi_0 T}\right), \tag{4}$$

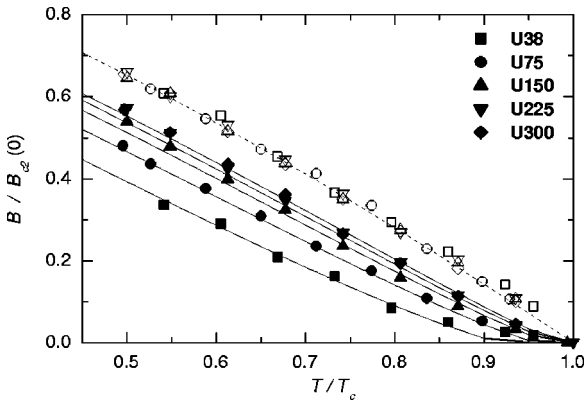

FIG. 3. Reduced phase diagram $B/B_{c2}(0)$ vs T/T_c, indicating upper critical field B_{c2} (open symbols) and melting field B_m (solid symbols), for all **U**-series samples. The dashed line follows from Eq. (4). The solid lines are the melting lines for the different samples according to 2D KT melting theory [Eq. (8)].

with Ψ the digamma function. In this relation $\xi(0)$ follows from

$$B_{c2}(0)=0.69ST_c=0.69\phi_0/[2\pi\xi(0)^2], \tag{5}$$

where $S=-dB_{c2}/dT|_{T=T_c}$ is the slope of $B_{c2}(T)$ close to T_c and the only free parameter. Figure 3 in combination with Table I shows that the experimentally determined $B_{c2}(T)$ values correspond very well to the theoretical relation for all samples if S is taken $S\approx 2$ T/K. This value for S is the same as values reported for a-Nb_3Ge in literature,[18] which is an indication that our determination of B_{c2} is correct. Also the values found for α correspond to values found earlier.

The 2D KT melting field B_m is the field above which the vortex lattice is in the liquid state and therefore unstable to the proliferation of dislocations. Below B_m the vortex lattice is frozen. The 2D KT melting criterion is

$$\frac{Ac_{66}a_0^2d}{k_BT}=4\pi, \tag{6}$$

where c_{66} is the shear modulus and A is a renormalization factor of the shear modulus c_{66} due to nonlinear lattice vibrations and vortex lattice defects as, e.g., bound edge-dislocation pairs, $A\approx 0.64$. The expression for c_{66} is

$$c_{66}=\frac{B_c(t)^2}{4\mu_0}b(1-0.58b+0.29b^2)(1-b)^2, \tag{7}$$

where $B_c(t)=B_{c2}(t)/\kappa_1\sqrt{2}$ and $\kappa_1=\kappa(1.25-0.25t)$, with $\kappa=3.54\times 10^4\sqrt{\rho_0 S}$. The distance between vortices is $a_0=1.075\sqrt{\phi_0/B}$. Finally, d is the thickness of the film. The melting curve is then given by

$$\frac{A\phi_0(1.07)^2d}{32\pi\mu_0k_B\kappa^2}\frac{B_{c2}(T)}{T(1.25-0.25t)^2}(1-0.58b_m+0.29b_m^2)\times(1-b_m)^2=1. \tag{8}$$

For the more strongly disordered samples of this work, it is not *a priori* clear if 2D KT melting takes place. A certain minimum correlated region is needed that may not exist in such disordered samples. It is also questionable if thermal depinning will not take place before melting. If we consider the $R_{ac}(B)$ measurements as given in Fig. 2, we see that R_{ac} does not drop sharply to zero below a certain field, because of a broad distribution in pinning potentials. Some vortices depin very easily and the low ac current is already strong enough to depin them. If 2D KT melting occurs, B_m has to correspond with the field at which partial flux flow begins in the $R_{ac}(B)$ measurements. Therefore B_m is determined from the measurements as indicated in Fig. 2 as the point where the linear regions go over into regions with a much less steep descent toward $R=0$.

A strong indication that the field we indicate as B_m actually corresponds to the melting field comes from a comparison with theory. The melting curve [Eq. (8)] has no free-fitting parameters, but is completely determined by T_c, S, ρ_0, and d. In Fig. 3 the experimentally determined values for $B_m(T)/B_{c2}(0)$ are plotted for all samples from the **U** series together with the calculated curves. Note that the experimentally determined B_m shift downward with decreasing d just as the calculated curves do. The correspondence between theory and experiment is quite good.

Figure 4(a) gives a double logarithmic plot of $V(I)$ for **U38** at $T=1.44$ K for a selected number of fields. In Fig. 4(b) the derived dynamic resistance $R_d(I)$ is plotted. At fields below $B_m\approx 1.8$ T the $V(I)$ curves do not bend downward as sharply as in weakly pinning samples. The critical current determined with a voltage criterion, $I_{c,V}$, is not well defined and depends on the actual number used. At high currents the $V(I)$ curves are linear with a constant R_d corresponding to the flux flow velocity R_f as calculated from the expression $R_f/R_n=1.1B/B_{c2}$.[1] This means all vortices are moving, but it takes large currents to achieve this. Only at a velocity as high as $v\sim 15$ m/s is full flux flow reached, compared to $v=0.2$ m/s to set all vortices in motion for very weakly pinning samples.[17] Of special interest are the data for $B=1.3$ T [see inset of Fig. 4(b)]. A small peak can be seen in R_d, which we ascribe to dynamic ordering, as will be discussed in Sec. V. At still higher currents an instantaneous transition to the normal state sets in, which is caused by the vortices reaching their critical velocity.[1] This transition is characterized by a peak in R_d with a maximum above the normal resistance R_n, as seen in Fig. 4 for the curve at $B=2.2$ T. Above B_{c2}, $R_d=R_n$, as the curve at $B=3.3$ T shows.

The critical current I_c can be determined from the full flux flow region of the $V(I)$ curves by extrapolating this linear part to $V=0$. In the inset of Fig. 4(a) the determination of I_c is indicated for $B=0.7$ T. The high velocities at which full flux flow is reached lead to high values for I_c. Another way to determine the critical current is by using a voltage criterion ($I_{c,V}$). However, due to the curved nature of $V(I)$, $I_{c,V}$ is not well defined and is much smaller than I_c determined by linear extrapolation. The difference can be an order of magnitude. For very weakly pinning samples the

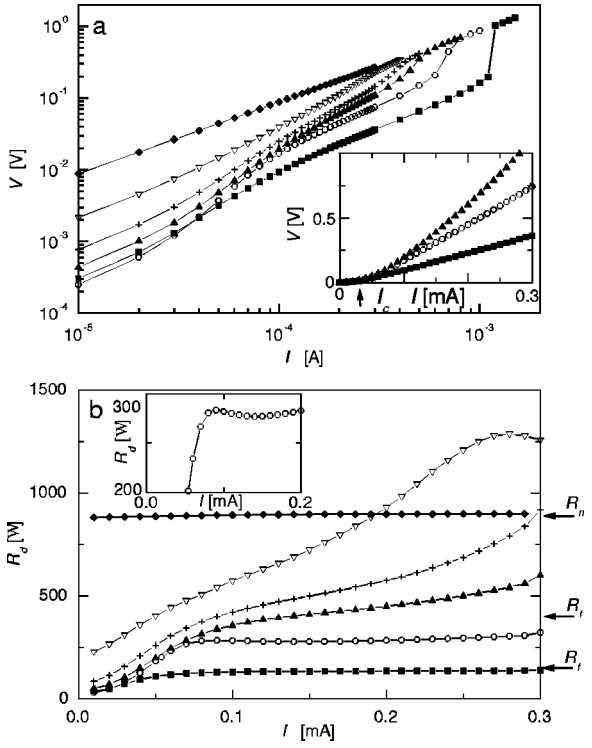

FIG. 4. (a) Double logarithmic plot of characteristic $V(I)$ for **U38** at $T \approx 1.44$ K. The fields are in counterclockwise direction $B = 0.7$, 1.3, 1.7, 1.9, 2.2, and 3.3 T. Inset: $V(I)$ on linear-linear scale for $B = 0.7$, 1.3, and 1.7 T. The determination of I_c for $B = 0.7$ is indicated. (b) $R_d(I)$ for **U38** at $T \approx 1.44$ K for the same fields as in (a) The normal resistance R_n and the flux flow resistance R_f at $B = 0.7$ T and $B = 1.3$ T are indicated. Inset: magnification of $R_d(I)$ at $B = 1.3$ T. The peak is associated with DO.

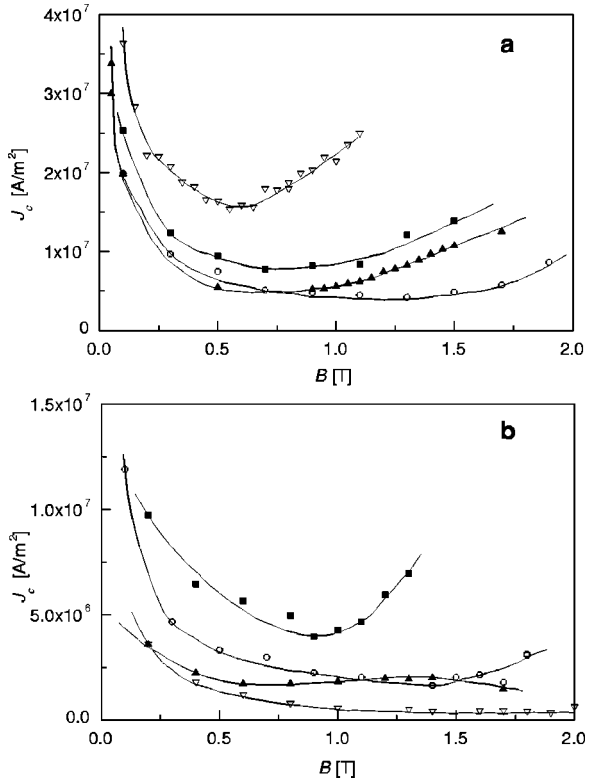

FIG. 5. (a) Critical current density J_c versus magnetic field B for **U**-series samples at 1.5 K: **U38** (squares), **U75** (circles), **U150** (up triangles), and **U225** (down triangles). Values of J_c for **U300** are larger than 4×10^7 A/m^2 at all fields and therefore not visible. (b) Critical current density J_c versus magnetic field B for **Z**-series samples at 1.5 K: **Z34** (squares), **Z67** (circles), **Z130** (up triangles), and **W190** (down triangles).

ratio between I_c and $I_{c,V}$ is only of the order of 2.[17] Here, I_c will be determined by extrapolation. Defined in this way, I_c is representative of the moving lattice and says something about the dynamic pinning. Figure 5 shows the critical current density J_c for the different sample series. The order of magnitude is 10^6 A/m^2 for the **Z** series to 10^7 A/m^2 for the **U** series.

The question is valid whether its behavior can be described by CP. That would already imply that the high-velocity motion is elastic, with few defects. In CP theory[1] the vortices start to move at $F_p = J_c \times B$ in bundles with volume $V_c = R_c^2 d$. The pinning force density in case of 2D CP can be written as

$$F_p = [W/R_c^2 d]^{1/2}, \tag{9}$$

where W is a parameter that describes the averaged pinning strength. W depends on the nature of the pinning centers and can differ between samples. Here we will not go into the exact nature of the pinning centers, but simply determine F_p experimentally. If the size of the correlated domains is determined by elastic deformations, R_c is given by

$$R_c = r_p c_{66} \left[\frac{8\pi d}{W \ln(w/R_c)} \right]^{1/2}, \tag{10}$$

where r_p is the range of the elementary pinning interactions, c_{66} is the shear modulus, and d and w are the sample thickness and width. R_c can be calculated by combining Eq. (10) with Eq. (9) and using the experimentally determined F_p. In case the size of the correlated domains is determined by plastic deformations, Eq. (10) for R_c is not valid anymore. This happens when R_c/a_0 drops below a certain criterion. Wördenweber, Kes, and Tsuei[20] showed that this criterion is $R_c/a_0 < 15$ when calculated from $J_{c,V}$. For R_c/a_0 calculated from J_c determined via linear extrapolation the criterion might be a different number. Further on we will see it is roughly $R_c/a_0 < 10$. From Eqs. (10) and (9) follows that in case of 2D CP, J_c at a certain field and temperature is proportional to $1/d$ for samples with the same pinning strength W.

From the experimentally determined $J_c(B)$, values for $R_c/a_0(B)$ were calculated using Eqs. (9) and (10). For $T = 1.5$ K they are shown in Fig. 6. The numbers reach the order of 5–30, and are higher for the **Z** series samples than for the **U**-series samples (Fig. 6). Also, for the **Z**-series a linear relation is found between J_c and $1/d$, as shown in Fig. 7 for $B = 0.5$ T, $T = 1.55$ K. This indicates that pinning strength and the pinning mechanisms are the same for the different thicknesses, and that the pinning is 2D CP. The three thinnest samples from the **U** series also show a linear

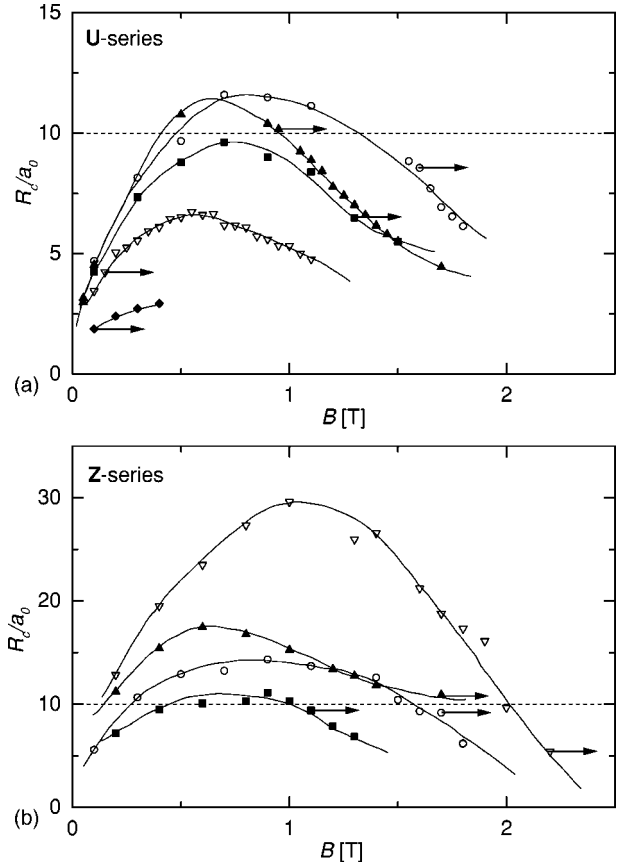

FIG. 6. (a) Correlated collective pinning length over intervortex distance R_c/a_0 vs B, calculated at $T=1.5$ K, for **U38** (squares), **U75** (circles), **U150** (up triangles), **U225** (down triangles), and **U300** (diamonds). The arrows indicate at which field value DO starts. (b) The same for **Z34** (squares), **Z67** (circles), **Z130** (up triangles), and **W190** (down triangles).

relation between $J_c(B=0.5$ T, $T=1.55$ K) and $1/d$, although with an offset at $1/d=0$, quite similar to the behavior found for films of $Mo_{79}Ge_{21}$.[11] The thicker films from the **U** series have much higher values of J_c. Whether the pinning

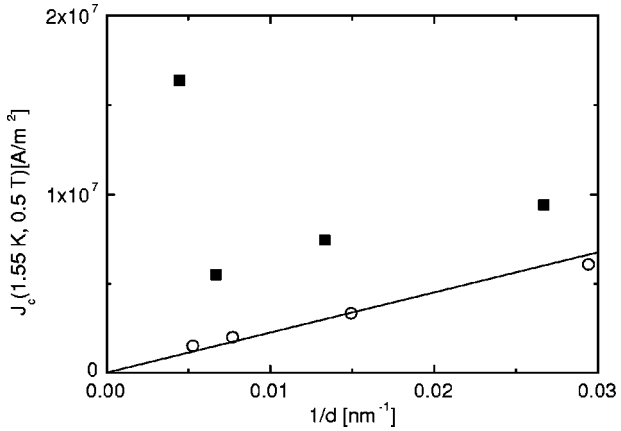

FIG. 7. Critical current density $J_c(B=0.5$ T, $T=1.55$ K) versus inverse thickness $1/d$ for all samples. Open symbols, **Z** series; filled symbols, **U** series.

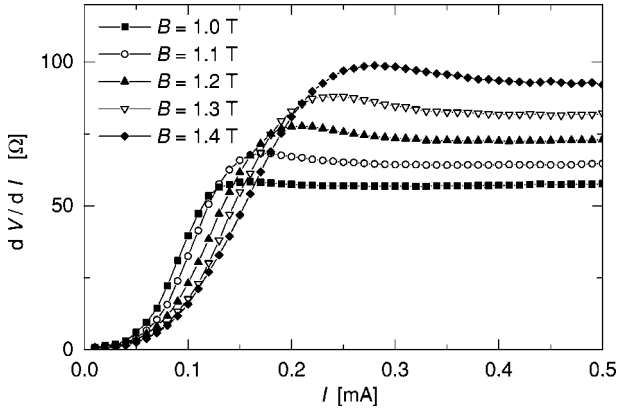

FIG. 8. Dynamic resistance R_d versus current I for **U150** at $T=1.55$ K. The fields are $B=1.0$, 1.1, 1.2, 1.3, and 1.4 T.

in these **U**-series samples is 2D CP cannot be determined from this analysis since W and the pinning mechanisms most likely vary.

Summarizing the sample characteristics, the samples presented in this work are more strongly disordered than the very weakly pinning samples of previous studies.[21,17] The larger disorder leads to channel-like, partial flux flow at the onset of motion, as $R(B)$ and $V(I)$ measurements show. B_{c2} can be determined from $R(B)$ and has values comparable to those of very weakly pinning samples. Dislocation-mediated melting still appears to take place: $B_m(T)$ is in good correspondence with the theoretical curve. The $V(I)$ measurements show that at high currents full flux flow occurs. From these high-current data, the critical current for the moving vortices has been determined. For the **Z** and **W** samples the pinning is certainly 2D CP and the size of the correlated domains is of the order $R_c/a_0\ 10-30$. For the **U**-series samples, it appears that the pinning mechanisms are not the same for different samples, but pinning might still be 2D CP with correlated domains of the order $R_c/a_0 \sim 5-12$. DO shows up in a number of the $R_d(I)$ curves as a peak, and this will be discussed next.

V. RESULTS ON DYNAMIC ORDERING

Figure 8 shows peaks in $R_d(I)$ at a number of fields for **U150** at $T=1.55$ K. At currents above the peak $R_d=R_f$. We associate the peaks with DO of the vortices as described in Sec. II. For all samples the (B,T) phase diagram has been scanned below the melting line down to $t\approx 0.5$ for occurrence of DO. In case of a peak in R_d the current at which the maximum occurs, I_p, has been determined.

Figure 9 shows the phase diagrams of **Z34** and **Z67** and of **U150** and **U225** ($w=100$ μm). Indicated by solid squares are the highest and lowest fields at which a DO peak in $R_d(I)$ was observed. The open squares indicate regions in which no DO was found. As can be seen in Fig. 9 a minimum field $B_{p,\mathrm{low}}$ exist below which DO does not occur. Also a maximum field appears to exists, above which no DO is observed. This is due to the fact that the small DO peak is masked by the onset of the much larger peak corresponding to the normal-state transition.

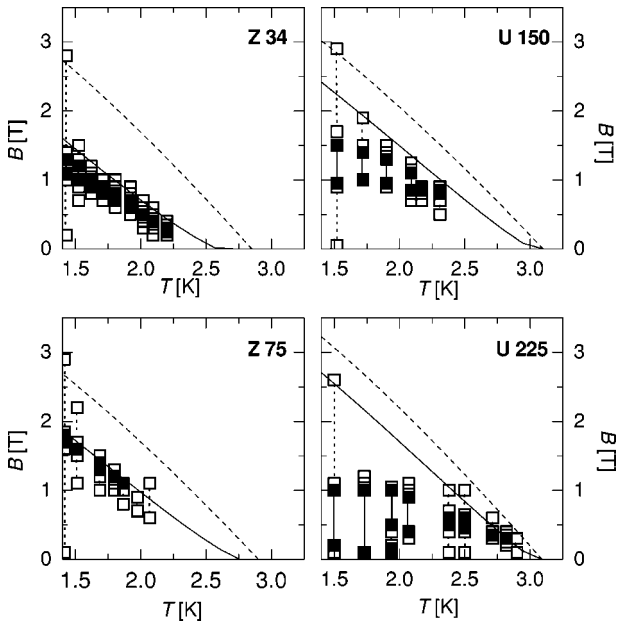

FIG. 9. (B,T) phase diagrams for **Z34**, **Z67**, **U150**, and **U225**. The dashed lines indicate $B_{c2}(T)$, the solid lines $B_m(T)$. The regions between the solid squares indicate at which fields DO has been observed. In the regions between open symbols, no DO has been observed.

The lowest field at which DO occurs shifts downward with increasing pinning. For the weaker pinning samples, especially those of the **Z** series, DO only occurs very close to the melting line. Above the melting line DO cannot occur and is never observed. Figure 10 shows the relation between the field at which DO first occurs, scaled on the melting field, $B_{p,\mathrm{low}}/B_m(t=T/T_c\approx 0.5)$, and a typical value for the critical current density $J_c(b=B/B_{c2}=0.3)$ taken as a measure for the intrinsic disorder. To relate DO to the disorder of the lattice in a different way, $B_{p,\mathrm{low}}$ is indicated in the graph of $R_c/a_0(B)$ (Fig. 6), giving the size of the 2D CP correlated regions. Although R_c/a_0 has been calculated from J_c of the moving vortices, it is also a measure for the disorder of the static lattice, since vortices in both the static and dynamic state are subject to the same pinning centers. As can be seen in Fig. 6, samples which are weakly enough disordered that R_c/a_0 reaches maximum values of the order of 10 or more only start to show DO as soon as R_c/a_0 drops below about 10 at the high-field side. For strongly disordered samples for which R_c/a_0 is of order 1 (**U225** and **U300**), DO already occurs at low fields.

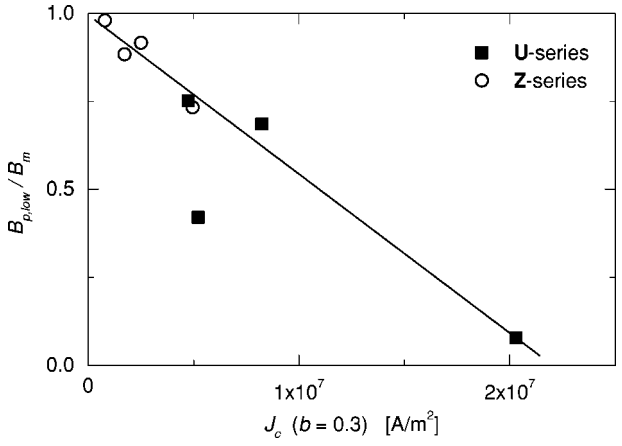

FIG. 10. Lowest field at which DO occurs $B_{p,\mathrm{low}}$ scaled on the melting field $B_m(T)$ versus the critical current $J_c(b=0.3)$ at $T=1.55$ K. The solid line is meant to guide the eye.

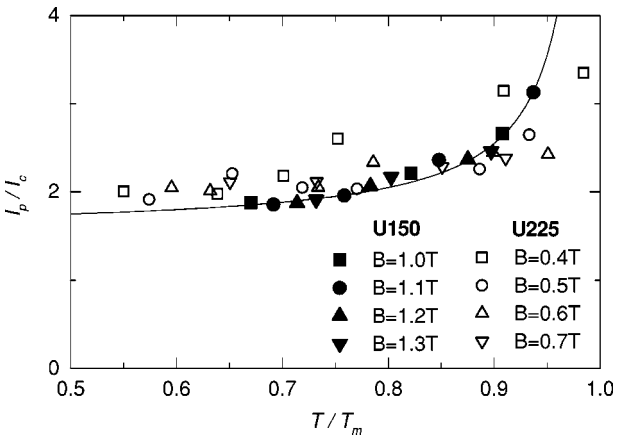

FIG. 11. Peak current over critical current I_p/I_c versus temperature scaled on the melting temperature T/T_m for **U150** (solid symbols) at fields of $B=1.0$ T (squares), 1.1 T (circles), 1.2 T (up triangles), and 1.3 T (down triangles) and for **U225** (open symbols) at $B=0.4$ T (squares), 0.5 T (circles), 0.6 T (up triangles), and 0.7 T (down triangles). The line is a fit to the relation $I_p/I_c=a+b/(1-T/T_m)$ with $a=1.55$ and $b=0.1$.

The currents I_p at which the maxima in $R_d(I)$ occur have been determined for the samples **U150** and **U225** as function of temperature at a number of fields. $I_p(T)$ increases for **U150**, but decreases for **U225** at all fields. However, if we plot I_p/I_c vs $t=T/T_m$ (Fig. 11), the ratio at low reduced temperatures is almost constant: $I_p/I_c\approx 2$, while close to $t=1$ all curves increase. For **U150** the curves of $I_p/I_c(t)$ at different fields ($B=1.0$, 1.1, 1.2, and 1.3 T) coincide. For T_m the value as calculated by the 2D KT melting theory has been used. Similar almost universal behavior is found for I_p/I_c vs $b=B/B_m$, as shown in Fig. 12 for all samples at t

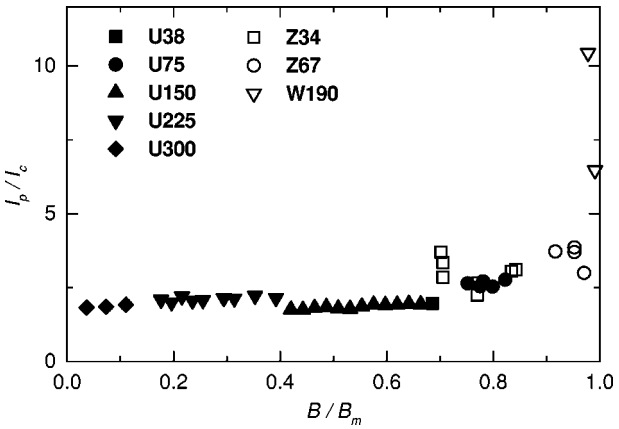

FIG. 12. Peak current over critical current I_p/I_c versus field scaled on the melting field $b=B/B_m$ for all samples at $t\approx 0.5$.

≈ 0.5. Up to $b \approx 0.8$ the value of $I_p/I_c \approx 2$ is constant. Close to $b=1$ this value starts to increase.

VI. DISCUSSION AND CONCLUSION

The results are in good qualitative agreement with the description of Faleski *et al.*,[8] discussed in Sec. II. Moreover, using the fact that even for quite high disorder 2D collective pinning theory and the concept of dislocation-mediated melting still can be used, the conditions for occurrence of DO can be quantified. The experiments show that if the intrinsic disorder of a sample is not too large, i.e., the correlated domains reach at least a maximum value of $R_c/a_0 \geqslant 10$, DO occurs when softening of the lattice increases the disorder. When at some field R_c/a_0 drops below 10, the disorder is large enough for DO to occur. The exact field at which this happens depends on the pinning and the maximum value of R_c/a_0. Therefore DO moves closer to the melting field for weaker pinning, and can lie so close to the melting field for very weakly pinning samples that it is hardly observable experimentally. The value of $R_c/a_0 \sim 10$ probably corresponds with the transition from an elastically to a plastically disordered lattice. At low fields, where R_c/a_0 is also small, DO does not occur, since the DO force F_{do} is lower than the pinning force F_p and the vortices order at the onset of motion. For samples with a large intrinsic disorder, i.e., R_c/a_0 of order 1 everywhere, DO already occurs at low fields, since the pinning force is now high and the lattice is plastically deformed also at low fields.

Considering the current values I_p at which DO takes place, we find a uniform ratio of peak and critical current I_p/I_c and similar behavior for all studied samples both as function of reduced temperature and reduced field: over a relatively large temperature and field range the ratio is constant, while close to the melting temperature or field it starts to increase. For the temperature dependence this is in qualitative agreement with the divergence of the driving force needed for DO as expressed in Eq. (1). For the field dependence, the underlying reason will be the same: near melting dislocations are more easily induced by the energy generated through the motion, and it takes larger velocities to suppress this effect. The comparison between experiment and theory can even be made more quantitative by realizing that, in the framework of 2DCP, Eq. (1) can be written in terms of the ratio I_p/I_c, since F_{do} corresponds with I_p and Γ with I_c. Specifically, we use the following relation between the disorder strength Γ of Eq. (1) and the average pinning strength W of Eq. (9): $\Gamma = W r_p^6 d$. This follows from realizing that Γ is a pinning *energy* squared times the area r_p^2 in which the pinning force acts while W is the pinning *force* squared per unit volume $r_p^2 d$. Writing Eq. (9) as $F_p = W/(r_p c_{66} d)$, using Eqs. (1) and (6), and the fact that $r_p \approx a_0/2$ close to T_m we find

$$\frac{F_{do}}{F_p} = \frac{I_p}{I_c} = \sqrt{\frac{\pi}{2}} \frac{A}{16} \frac{T_m}{T_m - T}. \tag{11}$$

The point of interest is that the ratio I_p/I_c diverges according to a universal constant, contrary to the divergence of I_p, which contains the sample-dependent parameters Γ and r_p. Fitting the data in Fig. 11 to the relation $I_p/I_c = a + b/(1 - T/T_m)$ yields $a = 1.55$ and $b = 0.1$. The latter value is to be compared to $\sqrt{\pi/2} A/16 \approx 0.05$, and the agreement is quite good. This also shows that the full description for DO behavior involves a crossover from a low-temperature (field) regime where the value of I_p/I_c is determined by the pinning parameters of the sample, to a high-temperature (field) regime where this is not the case, with the crossover temperature (field) again determined by the pinning. Coming back once more to the experiments of Hellerqvist *et al.*,[9,10] those are clearly below the crossover: although I_p diverges, I_p/I_c is actually going down in their whole temperature regime and the universal constant cannot be extracted from those data.

VII. SUMMARY

We have investigated dynamic ordering effects in films with varying amount of pinning and a two-dimensional vortex lattice. The nonlinear behavior of the voltage versus current relations, i.e., the peak in the dynamical resistance, indicates that current-induced ordering takes place. This DO only occurs if the disorder is large enough and a plastic flow region exists. The disorder depends on the intrinsic disorder of a sample, which is indicated by $J_c(b = \text{const})$ and on the field. A good measure for the disorder is the size of the correlated regions as determined using 2D collective pinning theory. DO appears if this size drops below the order of $R_c/a_0 \approx 10$. Since the field at which this happens depends on the intrinsic disorder of a sample, DO moves closer to the melting line for more weakly disordered samples. The current at which DO occurs scaled on the critical current is constant up to high reduced fields and temperatures and diverges at the melting transition, in agreement with the notion that increasing velocities are needed to overcome the effect of either temperature or softening of the shear modulus of the vortex lattice.

ACKNOWLEDGMENTS

This work was supported by the Nederlandse Stichting voor Fundamenteel Onderzoek der Materie (FOM).

*Permanent address: Dipartimento di Fisica and INFM, Università di Salerno, I-84081, Baronissi (Sa), Italy.

†Corresponding author. Email address: aarts@phys.leidenuniv.nl

[1] A. I. Larkin and Yu. N. Ovchinnikov, in *Nonequilibrium Superconductivity* (Elsevier Science Publishers, Amsterdam, 1986).

[2] P. H. Kes and C. C. Tsuei, Phys. Rev. Lett. **47**, 1930 (1981).

[3] P. H. Kes and C. C. Tsuei, Phys. Rev. B **28**, 5126 (1983).

[4] P. Koorevaar, J. Aarts, P. Berghuis, and P. H. Kes, Phys. Rev. B **42**, 1004 (1990).

[5] A.-C. Shi and A. J. Berlinksy, Phys. Rev. Lett. **67**, 1926 (1991).

[6] A. E. Koshelev and V. M. Vinokur, Phys. Rev. Lett. **73**, 3580 (1994).

[7] S. Scheidl and V. M. Vinokur, Phys. Rev. B **57**, 13 800 (1998).
[8] M. C. Faleski, M. C. Marchetti, and A. A. Middleton, Phys. Rev. B **54**, 12 427 (1996).
[9] M. C. Hellerqvist, D. Ephron, W. R. White, M. R. Beasly, and A. Kapitulnik, Phys. Rev. Lett. **76**, 4022 (1996).
[10] M. C. Hellerqvist and A. Kapitulnik, Phys. Rev. B **56**, 5521 (1997).
[11] F. Garten, W. R. White, and M. R. Beasly, Phys. Rev. B **51**, 1318 (1995).
[12] S. Bhattacharya and M. J. Higgins, Phys. Rev. Lett. **70**, 2617 (1993).
[13] A. Duarte *et al.*, Phys. Rev. B **53**, 11 336 (1996).
[14] U. Yaron *et al.*, Phys. Rev. Lett. **73**, 2748 (1994).
[15] W. Henderson, E. Y. Andrei, M. J. Higgins, and S. Bhattacharya, Phys. Rev. Lett. **77**, 2077 (1996).
[16] Y. Paltiel *et al.*, Nature (London) **403**, 398 (2000).
[17] P. Berghuis and P. H. Kes, Phys. Rev. B **47**, 262 (1993).
[18] M. H. Theunissen and P. H. Kes, Phys. Rev. B **57**, 3169 (1998).
[19] N. R. Werthamer, E. Helfand, and P. C. Hohenberg, Phys. Rev. **147**, 295 (1966).
[20] R. Wördenweber, P. H. Kes, and C. C. Tsuei, Phys. Rev. B **33**, 3172 (1986).
[21] P. Berghuis, A. L. F. van der Slot, and P. H. Kes, Phys. Rev. Lett. **65**, 2583 (1990).